Coupled Mode Theory Applied to Resonators in the Presence of Conductors

Sameh Y. Elnaggar, Richard J. Tervo, and Saba M. Mattar

***Abstract*—Using the method of images, Energy Coupled Mode Theory (ECMT), a coupled mode equation in the frequency domain, is extended to deal with important cases where resonators are in close proximity to conducting surfaces. Depending on the type of conductors and the orientation of the resonators, the method of images determines the relative phases of the images. Using the formed images, the coupled frequencies and fields can be determined by applying ECMT. Two cases are studied. In the first case, it is shown that a dielectric resonator inserted in a cavity couples with both the mirror image and the cavity. The frequency behavior is described by the interaction with the image which counteracts that with the cavity. The second case is that of resonators sandwiched between conducting plates. It is shown that an infinite array of stacked images is formed. The coupling of the resonator with its images determines the coupled frequencies and fields. In this context, the main advantage of ECMT is its ability to separate the effects of the walls from the uncoupled system. This means that the system parameters are independent of the separation distances and/or the type of conductors, which renders the post processing analyses easier and predictable. Provided that the behaviors of the uncoupled resonators are known, ECMT is general and can be applied to more complex systems.**

***Index Terms*—Coupled mode theory, coupled resonators, dielectric resonators, hybridization, metamaterials, perfect magnetic conductors (PMCs), split ring resonators.**

I. Introduction

PRACTICAL situations arise where resonators are installed in the proximity of conducting surfaces. For example, it was already shown that conducting plates affect the efficiency of power transfer via inductive-resonance coupling [1], [2]. Metamaterials can be realized by inserting split ring or dielectric resonators inside a waveguide operating below cutoff [3], [4]. Dielectric and loop gap resonators, used as probes in electron spin resonance spectroscopy, are usually housed in a shield or in a cavity [5]–[9]. In all of these situations, the frequencies and fields of the resonators are affected by the presence of nearby conductors.

Taking the influence of the conducting walls on the resonators was done by *ab initio* approaches. For example, this was done through out the derivation of the eigenmodes of two stacked dielectric resonators [10]–[12] which was based on the Cohn model [13]. For other resonators, such as loop gaps and split rings, analytical models are unavailable or are very complex, and one usually resorts to numerical techniques. The effect of the walls of a waveguide on a split-ring resonator was numerically and experimentally investigated using the coupling between the resonator and its mirror images. It was noted that a split-ring resonator trapped inside a waveguide couples with an infinite array of images [14].

To find the modes of an arbitrary number of coupled resonators, a coupled mode theory in the form of an eigenvalue problem was derived. The solution of the eigenvalue problem determines the coupled frequencies and fields [15]. Using the coupled mode equations, the eigenmodes of an electron spin resonance probe, which consists of a dielectric resonator inserted in a cavity center were found [7]. Other field-dependent parameters, such as the quality factor, the filling factor, and the resonator efficiency, were calculated [8], [9]. The same approach was generalized to explain the behavior of double split-ring resonators. The approach was considered to be a hybridization scheme which is the electromagnetic analog of molecular orbital theory. The determined modes are proven to obey the energy conservation principle and hence the eigenvalue equation was called energy coupled mode theory (ECMT) [15].

The fields of the coupled system, obtained by ECMT, are the linear superposition of those of the uncoupled modes. Therefore, an implicit assumption is that the tangential components of the electric (magnetic) fields of the uncoupled fields are negligibly small near perfect electric conductors (PMCs). Otherwise, the coupled modes severely violate the boundary conditions. In this paper, the method of images is combined with ECMT to extend its domain to cover situations where resonators are in the proximity of conducting surfaces. Hereafter, the method is named ECMT-I. To show the validity of the method, two cases are theoretically and numerically studied. The first is that of a dielectric resonator interacting with an enclosing cavity. In previous work, the interaction between the dielectric resonator and the cavity was studied where the dielectric resonator was installed in the cavity center and hence its field values are small near the walls [7], [8]. In the current work, the effect of the walls on the coupled frequencies is taken into account. The second case discusses resonators sandwiched between parallel

Manuscript received January 05, 2015; revised March 26, 2015 and May 08, 2015; accepted May 09, 2015. Date of publication June 01, 2015; date of current version July 01, 2015. The work of S. Y. Elnaggar was supported by the University of New Brunswick in the form of pre-doctoral teaching and research assistantships. The work of S. M. Mattar was supported by the Natural Sciences and Engineering Research Council of Canada through a discovery (operating) grant.

S. Y. Elnaggar is with the School of Engineering and Information Technology, University of New South Wales, Canberra, ACT, Australia.

R. J. Tervo is with the Department of Electrical and Computer Engineering, University of New Brunswick, Fredericton, NB E3B 5A3, Canada.

S. M. Mattar is with the Chemistry Department, University of New Brunswick, NB E3B 5A3, Canada (e-mail: mattar@unb.ca).

Color versions of one or more of the figures in this paper are available online at http://ieeexplore.ieee.org.

Digital Object Identifier 10.1109/TMTT.2015.2432766

plate conductors. This broad class of problems covers the presence of resonators inside waveguides which can find applications in filters and metamaterial based devices. It also proposes an analytical apparatus to study the behavior of coupled resonators, such as inductively coupled resonant coils, in the presence of conductors [1], [2].

This paper is organized as follows. Section II discusses the method of images, the concept of the *image resonator* and its integration with the coupled system. Expressions for the frequency shifts for dielectric and split-ring resonators near a conducting plane are derived. Similarly, the case of resonators sandwiched between two conducting plates is discussed. In Section III, two configurations are numerically solved and compared with finite element simulations and other independent analytical models. Using ECMT-I, the numerical results are explained based on the uncoupled parameters (frequencies and fields) which render the analysis simpler and more intuitive. Finally, the conclusions follow in Section IV.

II. Theory

When losses are negligibly small, the frequency and fields distributions of the modes of a resonator can be obtained by solving the eigenvalue problem

$$\nabla \times \frac{1}{\mu_r(\mathbf{r})} \nabla \times \mathbf{E}(\mathbf{r}) = \frac{\omega^2}{c^2} \epsilon_r(\mathbf{r}) \mathbf{E}(\mathbf{r}), \ \mathbf{r} \in \mathcal{D} \qquad (1)$$

over the domain boundary $\partial\mathcal{D}$, subject to the suitable boundary conditions. Here, $\mathbf{E}$ is the electric field, $\epsilon_r(\mathbf{r})$ is the relative permittivity, $\mu_r(\mathbf{r})$ is the relative permeability, and $\omega = 2\pi f$ is the resonant angular frequency. The boundary can be divided into three main types: 1) perfect electric conductor (PEC), where the tangential $\mathbf{E}$ component vanishes; 2) PMC, where the tangential $\mathbf{H}$ component vanishes; and 3) infinity (radiation), where the magnitude of the fields are zero ($\mathbf{E}, \mathbf{H} \to 0$ whenever $\mathbf{r} \to \infty$).

Consider the structure shown in Fig. 1(a), which represents a resonator in the proximity of a conducting plane (either PEC or PMC). If the upper half space is only considered, Fig. 1(b) represents an equivalent problem. Both boundary value problems give the same results in the upper half space. This equivalency is used in full-wave solvers to reduce the problem space. In this case, the original system is the one in Fig. 1(b), and the introduction of the suitable boundary (symmetry plane) cuts the space in half and hence reduces the computational time.

ECMT is also in an eigenvalue problem form. However, unlike (1), the operator relies on the fields of the interacting resonators and hence the problem space is limited to the number of resonators. Thus, one can start from the configuration given in Fig. 1(b) to determine the mode of interest of the structure depicted in Fig. 1(a). In general, the two modes of the resonators in Fig. 1(b) interact, resulting in a symmetric and an anti-symmetric modes. Depending on the conductor type (PEC or PMC), each mode will represent a solution to the system in Fig. 1(a). Once the modes of a resonator/conducting plane system are determined, ECMT can be reapplied to study their interactions with other nearby resonators. It is crucial to note that the solution of the structure in Fig. 1(a) is a subset of the one shown in Fig. 1(b). The right solution is singled out by the theory of images.

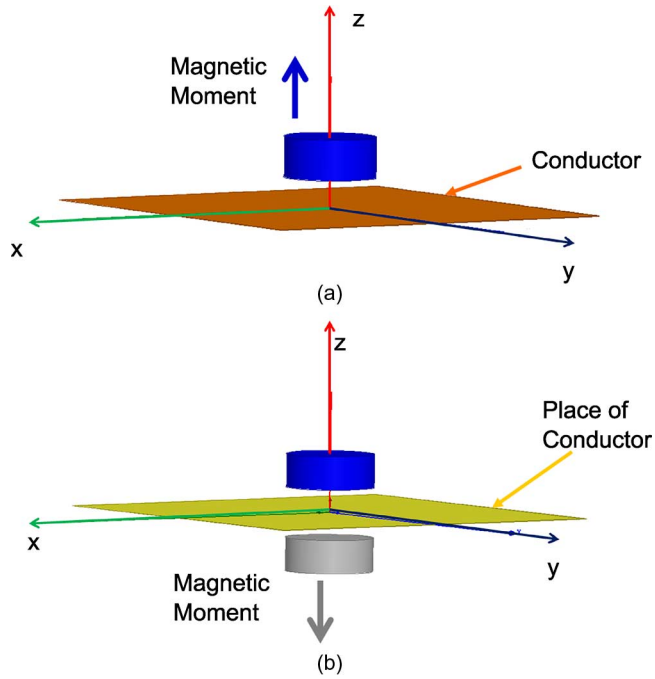

Fig. 1. Typical structure of a dielectric resonator interacting with a conducting plane. (a) Original system. (b) Equivalent structure where the plane is replaced by an equivalent image resonator.

The orientation of the resonator with respect to the conducting plane is crucial in determining the right coupled mode behavior. For example, consider a cylindrical dielectric resonator close to a PEC as shown in Fig. 1(a). The dielectric resonator's $TE_{01\delta}$ mode behaves like a magnetic dipole where its direction is shown in Fig. 1 [13]. According to the image theory, the real and image resonators have anti-parallel dipole moments, which are both normal to the conducting plane [16]. Therefore, the electric fields of both resonators are 180° out of phase which guarantees that the tangential component of the electric field vanishes on the mid plane. Using coupled mode theory, the coupling coefficient κ is found to be proportional to $\int_{V_{DR}} \mathbf{E}_1 \cdot \mathbf{E}_2 dv$, where the integration is carried over one of the dielectric resonators volume V_{DR} [24]. Since $\mathbf{E}_1$ and $\mathbf{E}_2$ are anti-parallel, κ is negative. The frequency of the symmetric mode is [7]

$$f^{++} = f_0 \sqrt{1 - \kappa(2s)} \qquad (2)$$

where f_0 is the frequency of the dielectric resonator in free space (hereafter called the uncoupled frequency) and $\kappa(2s)$ is the coupling coefficient at double the distance between the resonator and the conducting plane. Thus, the effect of the PEC is to increase the frequency of the mode.

On the other hand, if a split-ring resonator is brought close to a PEC wall, as shown in Fig. 2, image theory dictates that the magnetic dipole moments of the resonator and its image are parallel to each other and to the conducting plane as shown in Fig. 2 [16]. Again, the frequency of the symmetric mode is given by (2). Now κ is proportional to $\int_V (\mu_0 \mathbf{H}_1 \cdot \mathbf{H}_2 - \epsilon_0 \mathbf{E}_1 \cdot \mathbf{E}_2) dv$ [24]. Because the magnetic moments are parallel, the first term is positive. Moreover, to preserve the parallelism of the magnetic dipoles, the electric fields, concentrated in the vicinity of

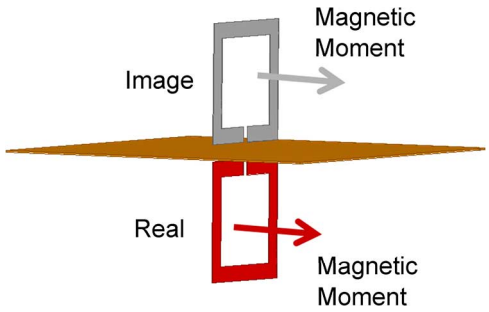

Fig. 2. Split-ring resonator is coupled to its image in the symmetric mode.

the gaps are anti-parallel (i.e, $\int_V \mathbf{E}_1 \cdot \mathbf{E}_2 dv \leq 0$) and hence κ is positive. Thus, the resulting mode has a frequency f^{++} which is lower than the uncoupled frequency f_0. This interpretation, based on coupled mode theory, explains why the frequency decreases when the gap of the split-ring gets close to the waveguide wall. Zhang *et al.* attributed this to the increase in gap capacitance [14].

As already mentioned, resonators sandwiched between two parallel plates are not uncommon. For example, metamaterials can be realized inside a waveguide by inserting dielectric or split ring resonators. Each resonator forms a unit cell which interacts with its neighbors and with the mirror images. The cylindrical cavity resonance technique, a method used to measure the dielectric properties of a material, is another example [17]. In this method, the dielectric sample is placed inside a cylindrical cavity which has a diameter at least double that of the sample. The unloaded Q_u, the central frequency, the 3-dB bandwidth, and the transmission coefficient (S_{21}) are used to determine the sample's loss tangent $(\tan\delta)$. For samples which have relatively low permittivity values, the walls of the cylindrical cavity can have a significant effect. Moreover, the cavity modes can interact with the dielectric $TE_{01\delta}$ mode [7], [8]. The efficiency of wireless power transfer via strong inductively-coupled resonant coils can also be affected by metallic planes [1], [2]. To understand the behavior of such complex systems, it is imperative to model the simplest cases: one and two resonator(s) installed between two parallel plates.

For the case of a resonator sandwiched between two conducting planes, as shown in Fig. 3, the equivalent coupled mode structure is an array of infinite number of images [14]. Ignoring the coupling induced frequency shift terms, the eigenvalue problem of the coupled system can be written as [15]

$$\omega_0^2 \begin{pmatrix} 1 & -\kappa_{12} & -\kappa_{13} & \cdots & -\kappa_{1n} & \cdots \\ -\kappa_{21} & 1 & -\kappa_{23} & \cdots & -\kappa_{2n} & \cdots \\ \vdots & \vdots & \ddots & \vdots & \vdots & \vdots \\ -\kappa_{m1} & -\kappa_{m2} & \cdots & 1 & -\kappa_{mn} & \cdots \\ -\kappa_{n1} & -\kappa_{n2} & \cdots & -\kappa_{n(n-1)} & 1 & \cdots \\ \vdots & \vdots & \vdots & \vdots & \vdots & \ddots \end{pmatrix} \underline{a} = \omega^2 \underline{a}$$
$$\underline{a} = (a_1\ a_2\ \cdots)^\top \tag{3}$$

where ω_0 is the angular frequency of the uncoupled resonator, κ_{ij} is the coupling coefficient between the ith and jth resonators, a_i is the expansion coefficient of the i^{th} resonator, and ω is the frequency of the coupled system. κ_{ij} can be calculated

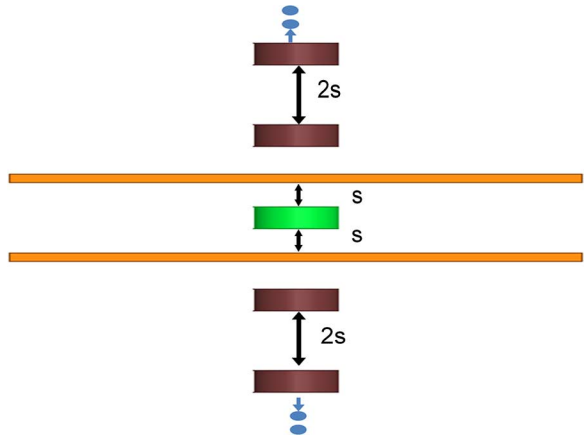

Fig. 3. One resonator between two conducting planes. An equivalent system: instead of the conducting planes, an infinite chain of image resonators can be placed all separated by 2s.

using the overlap integrals [7], [24] or the frequency splitting formula $\kappa_{ij} = (\omega_{+-}^2 - \omega_{++}^2)/(\omega_{+-}^2 + \omega_{++}^2)$, where ω_{++} and ω_{+-} are the angular frequencies of the symmetric and anti-symmetric modes, respectively. As will be shown, both methods were used in the current article. It is worth noticing that, although (3) has infinite number of eigenvectors, only one of them satisfies the boundary conditions at the position of the conducting plane. Because the relative phases of the images are taken into account in constructing the matrix in (3), this eigenvector is always the first one, where its components have the same sign.

Fortunately, the coupling coefficient decreases sharply as the distance between the resonators increases. Therefore, the coupling coefficient between adjacent neighbors is considered only. Consequently, (3) simplifies to

$$\omega_0^2 \begin{pmatrix} 1 & -\kappa & 0 & \cdots & 0 & \cdots \\ -\kappa & 1 & -\kappa & \ldots & 0 & \cdots \\ \vdots & \vdots & \ddots & \vdots & \vdots & \vdots \\ 0 & \cdots & -\kappa & 1 & -\kappa & \cdots \\ 0 & 0 & \cdots & -\kappa & 1 & \cdots \\ \vdots & \vdots & \vdots & \vdots & \vdots & \ddots \end{pmatrix} \underline{a} = \omega^2 \underline{a}. \tag{4}$$

In (4), the subscripts of κ_{ij} were dropped since all coupling coefficients between nearest neighbors are equal. Since the matrix is symmetric and tri-diagonal, the first eigenvalue approaches [18]

$$\omega^2 = \omega_0^2(1 - 2\kappa). \tag{5}$$

The corresponding eigenvector is [18]

$$a_m = \lim_{N\to\infty} \sin\frac{(N-m+1)\pi}{2N+2}, \qquad m = 0, 1, 2, \ldots N. \tag{6}$$

m is the image order which, as shown in Fig. 4, is zero for the original resonator. Image pairs are labelled according to their position from the original resonator. N is the number of image pairs which tends to infinity when all pairs (orders) are taken into account. In (6), the eigenvectors are normalized such that the coefficient of the original resonator (Zeroth order) a_0 is set

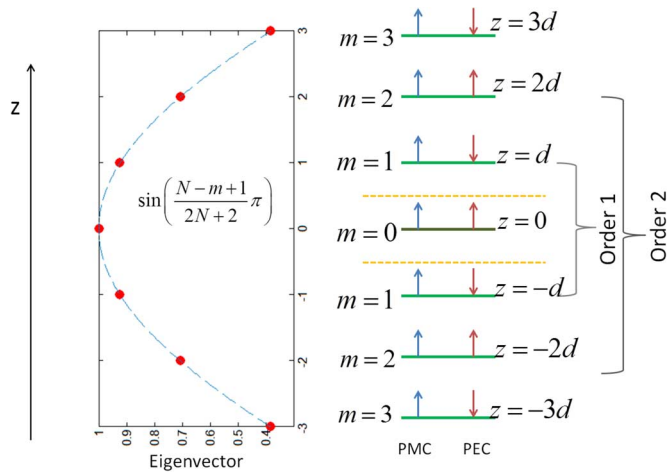

Fig. 4. Resonator sandwiched between two conducting planes. For PEC walls, the phases of the images are alternating. For the PMC walls, all the images have the same phase of the original resonator. The left hand side shows the magnitude of the a_m coefficients compared to a_0 which is normalized to unity.

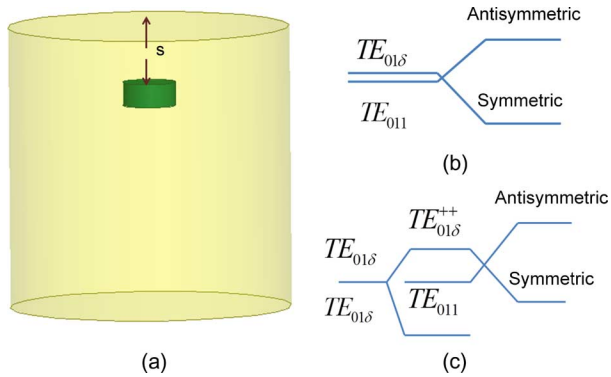

Fig. 5. (a) Dielectric resonator allowed to move along its common axis with the cavity. The holder is of low loss and low permittivity material. It is therefore not shown. Conceptual view of the hybridization between the modes: (b) when the image is not taken into account and (c) when the image is taken into account.

to 1. It is worth noticing that the lower the image order (closer to the real resonator), the more its contribution to the system behavior (higher a_m value).

In this paper, the following notation is used to represent resonators sandwiched between conducting planes: the resonator is represented by "$\mathcal{R}$" and PEC wall as "|". Because of their resemblance to high-impedance surfaces [19], "$\sqsubset$" or "$\sqsupset$" are used to represent a PMC wall. For example, a resonator sandwiched between two PMC walls is denoted by "$\sqsubset\ -\mathcal{R}-\ \sqsupset$". Two resonators sandwiched between two PEC walls are represented by "$|-\mathcal{R}-\mathcal{R}-|$".

For a resonator sandwiched between two PEC walls ($|-\mathcal{R}-|$), the magnetic dipole moment of any two consecutive resonators p and $p+1$ are anti-parallel, i.e., $\kappa<0$. This guarantees that the electric field vanishes on the walls. On the contrary, all moments are parallel ($\kappa>0$) for $\sqsubset\ -\mathcal{R}-\ \sqsupset$.

The total electric field $\mathbf{E}$ is the vector sum of the fields, $\mathbf{E}_m$ of all orders. Thus

$$\mathbf{E}(\mathbf{r})=\mathbf{E}_0(\mathbf{r})+\lim_{N\to\infty}\sum_{m=1}^{N}a_m\mathbf{E}_m(\mathbf{r}) \tag{7}$$

where

$$\mathbf{E}_m(\mathbf{r})=(-1)^{m+1}\left[\mathbf{E}_0(\mathbf{r}-\hat{z}md)+\mathbf{E}_0(\mathbf{r}+\hat{z}md)\right] \tag{8}$$

for $|-\mathcal{R}-|$ and

$$\mathbf{E}_m=\left[\mathbf{E}_0(\mathbf{r}-\hat{z}md)+\mathbf{E}_0(\mathbf{r}+\hat{z}md)\right] \tag{9}$$

for $\sqsubset\ -\mathcal{R}-\ \sqsupset$. d is distance between the two planes.

III. Results and Discussion

A. Dielectric-Cavity Interaction

The coupling between a dielectric resonator and a cavity was previously studied [7], [20]. It was shown that inserting a dielectric resonator in a cavity improves the signal to noise ratio of an electron spin resonance probe [9]. Adding another dielectric resonator, linearly changes the frequency of the desired mode as a function of the separation distance between the two dielectric resonators. This *nice* linear response was used to tune the frequency over a wide range. However once they are close to the cavity walls, the benefit of using the dielectric resonators is lost and thus putting a limitation on the maximum separation distance and consequently the frequency spanning range. [21]. The apparent *loss* of the dielectric effect on the probe performance was explained by using boundary conditions arguments where the fields diminish due to the simultaneous presence of perfect electric and perfect magnetic walls. In the analysis that was carried out in [7]–[9], only one dielectric resonator was used and it was installed at the cavity center. Hence, it was far away from the cavity walls and its interaction with the images was negligibly small. Therefore it was justifiable to calculate the coupling coefficient between the dielectric and the cavity using the dielectric $TE_{01\delta}$ and the cavity TE_{011} modes only [2]. The two modes couple to give two modes: *symmetric* and *anti-symmetric*. However, if the dielectric was brought close to one of the walls, as shown in Fig. 5, the coupling with the image becomes significant and cannot be ignored.

Here, ECMT-I will be used to calculate the effect of the cavity walls on the resonant frequencies of the symmetric and anti-symmetric modes. A dielectric resonator ($\epsilon_r=29.2$, diameter $=$ 6 mm, height $=$ 2.65 mm) is inserted into a cylindrical cavity (hiameter $=$ height $=$ 4.1 cm). These dimensions guarantee that the resonant frequencies of the $TE_{01\delta}$ and TE_{011} modes are equal (9.7 GHz). For different distances s, the frequencies of both the symmetric and the anti-symmetric modes are calculated using ECMT [15] and ECMT-I and compared with HFSS (Ansys Corporation, Pittsburgh, PA, USA) eigenmodes simulations. Fig. 5(b) and (c) presents a conceptual view of the hybridization of the cavity TE_{011} and the dielectric mode. In Fig. 5(b), when the effect of the image is neglected, the TE_{011} mode couples with the dielectric $TE_{01\delta}$ mode. As a result, two coupled modes, the symmetric and anti-symmetric, arise. Fig. 5(c) shows a two stage hybridization scheme. Here the dielectric $TE_{01\delta}$ mode couples with its own image, which is 180° out of phase. Consequently, the resulting mode, the $TE^{++}_{01\delta}$, then couples with the cavity TE_{011} mode

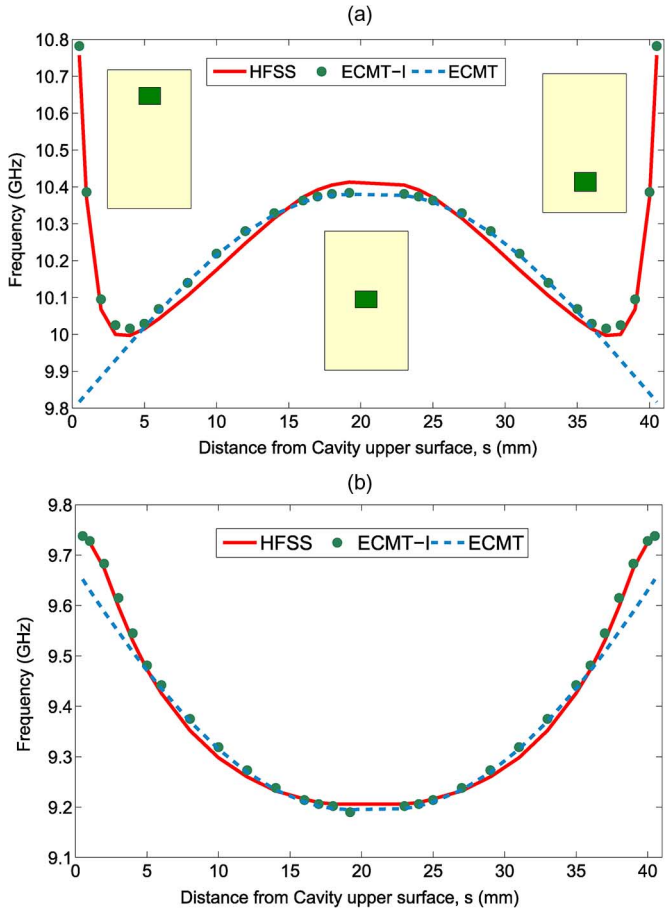

Fig. 6. Coupled frequencies calculated using ECMT, ECMT-I, and HFSS. (a) Anti-symmetric mode. (b) Symmetric mode. In (a), the insets depicts descriptive scenarios of the position of the dielectric resonator in the cavity.

yielding two coupled modes: symmetric and antisymmetric. The coupling between the cavity on one hand and the dielectric or the dielectric-image pair on the other is determined as in [7] using the overlap integrals of the electric fields inside the dielectric material. Here, the fields expressions of the $TE_{01\delta}$ mode are obtained using the Cohn model which, as shown in [7], provides accurate field values inside the dielectric material. Because diffraction is not taken into account, the accuracy of the electric field is lost outside the dielectric material where the fields are evanescent [23]. Thus the Cohn model does not provide the accuracy needed to compute the frequency of the dielectric-image pair which, unlike the coupling between the dielectric resonator and cavity, strongly relies on the evanescent fields. Hence, HFSS eigenmode solver is used to determine the frequency of the dielectric-image pair. This value is then plugged into the ECMT eigenvalue problem together with the electric field expression of the dielectric-image pair which is given by $\mathbf{E}' = (\mathbf{E}(x,y,z) - \mathbf{E}(x,y,z-2s))/\sqrt{(2)}$, where $\mathbf{E}$ is the electric field of the $TE_{01\delta}$ mode.

Fig. 6 shows how the frequencies change as a function of s. As the figure presents, incorporating the method of images gives more accurate results particularly for the anti-symmetric mode. This can be explained by noting that in order to calculate the frequencies, ECMT uses the $TE_{01\delta}$ mode, while ECMT-I uses the $TE_{01\delta}^{++}$ mode which, by referring to (2) and noting that $\kappa < 0$, has a higher frequency value. When the dielectric is close to the wall, the electric field of the cavity's TE_{011} mode is small ($\mathbf{E} \propto \cos(\pi z/d)$) [8]. The coupling coefficient κ is the overlap of the electric fields of the cavity and the dielectric resonator and hence is small close to the wall. This means that the modes tend to decouple. The symmetric mode tends to the cavity TE_{011} mode [6] and the anti-symmetric mode approaches the dielectric $TE_{01\delta}$ mode (ECMT used) or $TE_{01\delta}^{++}$ mode (ECMT-I used). When the dielectric resonator is very close to the wall, the frequency of the $TE_{01\delta}^{++}$ can be significantly higher than that of the $TE_{01\delta}$. This explains why ECMT completely fails to explain the behavior of the anti-symmetric mode depicted in Fig. 6(b).

Similarly, the minimum of the anti-symmetric mode in Fig. 6(b) can be explained by noting that it is the result of two opposing actions: 1) the decrease in the frequency due to the coupling with the cavity and 2) the increase in frequency due to the coupling with the image. It is expected that the dielectric $TE_{01\delta}$ mode couples with other cavity modes. However, the contribution of their quantitative effect is very small [7]. It is also expected that the discrepancy between HFSS and ECMT-I results will decrease if a more sophisticated model for the dielectric mode was used.

B. Resonator Between Two Parallel Plates

Because an analytical model, based on the Cohn model, is already available, a dielectric resonator is considered. Regardless of the limitations of the Cohn model, it provides deep insight into the coupling mechanism and allows the finding of closed form expressions. However, the general analysis and findings are valid for any type of resonators. The coupled (coupling with the images) frequencies and fields are calculated and compared to the values obtained using the analytical model. As mentioned in Section II, the resonator symmetrically couples with the stack of infinite images. The coupled, denoted by $TE_{01\delta}^{+++\cdots}$, has a frequency of

$$f_{TE_{01\delta}^{+++\cdots}} = \sqrt{1-2\kappa(d)}f_0, \begin{cases} \kappa < 0, & \text{for } |-\mathcal{R}-| \\ \kappa > 0, & \text{for } \sqsubset -\mathcal{R}- \sqsupset \end{cases} \tag{10}$$

where d is the separation distance between the conducting planes. The frequency given by (10) is calculated for different separations. The results are then compared with the values obtained using the analytical model [11]. For the sake of completeness, the analytical models of both $|-\mathcal{R}-|$ and $\sqsubset -\mathcal{R}- \sqsupset$ are presented in the Appendix. The frequency values are plotted in Fig. 7 for a dielectric resonator ($\epsilon_r = 29.2$, diameter $=$ 6 mm, height $=$ 2.65 mm) inserted between two plates which are separated by a distance $d =$ 3.15–8.65 mm.

Although (10) is much simpler than the transcendental equations (18) and (19) (see the Appendix), ECMT-I gives very accurate values when $d >$ 4 mm (refer to Fig. 7). Unlike the analytical model, ECMT-I *separates* the effects of the walls from the resonator's uncoupled frequency (f_0). The contribution of the walls is lumped in κ. For $d <$ 4 mm, the discrepancy between the two methods can be attributed to: 1) the frequency expression (2) was determined based on the nearest neighbor interactions only and 2) when the resonators are close, coupling-induced frequency shifts are not negligible. Coupling-induced frequency shifts change the on-diagonal terms and hence shift the

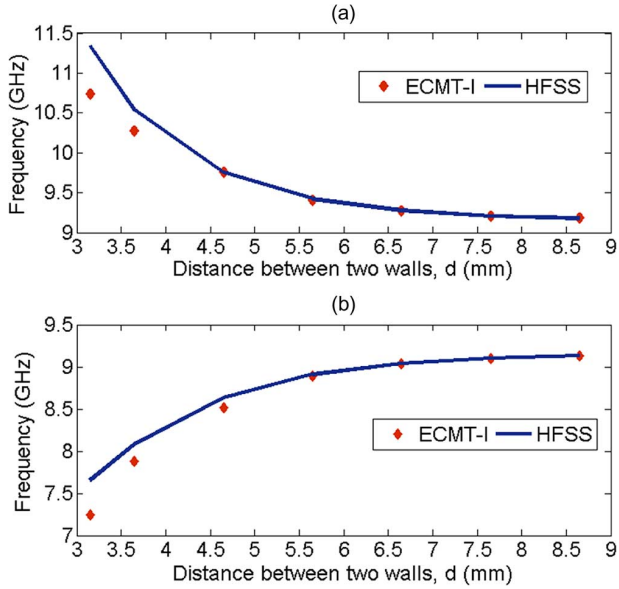

Fig. 7. Frequency of the resonant mode for a dielectric resonator sandwiched between two conducting planes. (a) PEC. (b) PMC.

frequencies [15], [22]. This shift in frequency can be attributed to the proximity effects of the other resonators. The presence of other resonators has the effect of changing the equivalent self capacitance and inductance and thus changing the on-diagonal terms. This behavior is different from the coupling behavior which introduces mutual capacitances and/or inductances.

In the following, expressions for the coupled electric field $\mathbf{E}$ will be derived and compared with the field expression (22). The electric field of the $TE_{01\delta}$ mode, centered at the origin, can be written as [23]

$$\mathbf{E}_0 = -k_\rho J_0(k_\rho r) \begin{cases} \cos k_1 z, & |z| < \frac{h}{2} \\ \cos k_1 \frac{h}{2} e^{-k_2\left(z-\frac{h}{2}\right)}, & |z| > \frac{h}{2} \end{cases} \hat{\boldsymbol{\phi}}. \quad (11)$$

$\mathbf{E}_0$ is in the azimuthal direction $\hat{\boldsymbol{\phi}}$. h is the dielectric height, k_ρ is the radial wave number, k_2 is the axial free space attenuation factor and k_1 is the propagation constant inside the dielectric. Using ECMT-I, the total electric field $\mathbf{E}$ can be determined by (7) and (8) or (9). Equation (7) separates the fields of the uncoupled resonator $\mathbf{E}_0$ from the contributions of the conductors $\{\mathbf{E}_m\}_{m=1}^{\infty}$. For the dielectric resonator, the field of the mth pair, $\mathbf{E}_m$, is found to be

$$\begin{aligned} \mathbf{E}_m =& 2 \cdot (-1)^{m+1} k_\rho J_1(k_\rho r) e^{-k_2(md-h/2)} \\ & \times \cos(k_1 h/2) \cosh(k_2 z) \hat{\boldsymbol{\phi}} \end{aligned} \quad (12)$$

for $|-\mathcal{R}-|$ and

$$\mathbf{E}_m = -2 \cdot k_\rho J_0(k_\rho r) e^{-k_2(md-h/2)} \cos(k_1 h/2) \cosh(k_2 z) \hat{\boldsymbol{\phi}} \quad (13)$$

for $\sqsubset -\mathcal{R}- \sqsupset$. Expressions (6), (12) and (13) are substituted back into (7), and the field correction $\hat{\mathbf{E}} = \sum_{m=1}^{\infty} a_m \mathbf{E}_m$ simplifies to

$$\hat{\mathbf{E}} = 2k_\rho J_0(k_\rho r) \cos(k_1 h/2) \cdot \left(\frac{e^{-k_2(d-h/2)}}{1+e^{-k_2 d}} \right) \cdot \cosh(k_2 z) \hat{\boldsymbol{\phi}} \quad (14)$$

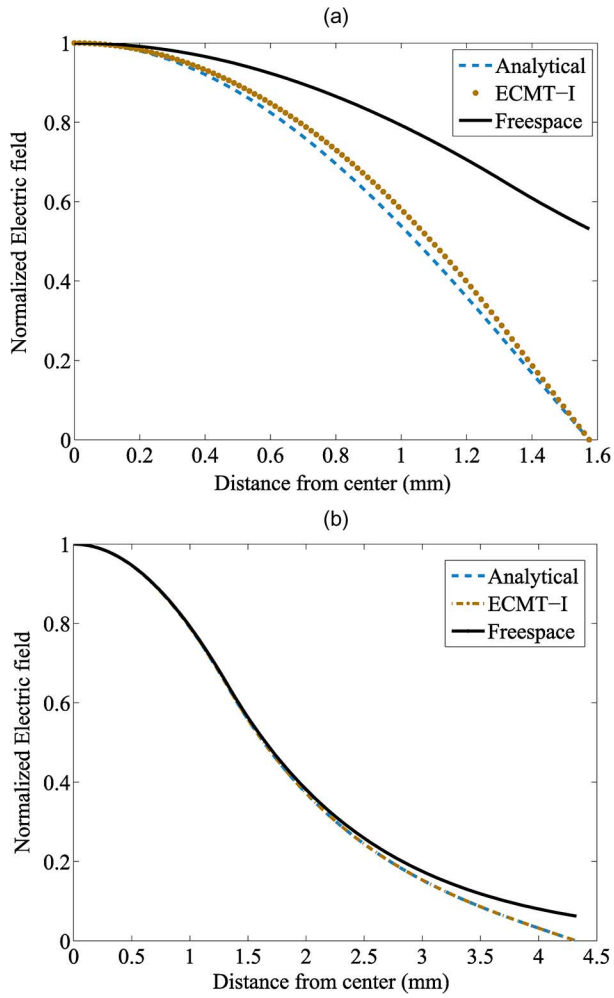

Fig. 8. Dielectric resonator sandwiched between two PEC plates: The normalized electric field calculated over $z \in [0, d/2]$. The distance between the two plates d is (a) 3.15 mm and (b) 8.65 mm.

for $|-\mathcal{R}-|$ and

$$\hat{\mathbf{E}} = -2k_\rho J_0(k_\rho r) \cos(k_1 h/2) \cdot \left(\frac{e^{-k_2(d-h/2)}}{1-e^{-k_2 d}} \right) \cdot \cosh(k_2 z) \hat{\boldsymbol{\phi}} \quad (15)$$

for $\sqsubset -\mathcal{R}- \sqsupset$.

Expressions (14) and (15) are calculated over $z \in [0, d/2]$ and compared with the analytical model [cf. (22)–(26)]. The results are plotted in Figs. 8 and 9. It is apparent that ECMT-I gives very accurate values of $\mathbf{E}$. Other than this, ECMT-I *separates* the conductors' effects, $\hat{\mathbf{E}}$ from the uncoupled field, $\mathbf{E}_0$. Moreover, the parameters k_1 and k_2 depend on the uncoupled resonance frequency and is independent of the separation distance d. This means that $\hat{\mathbf{E}}$ explicitly depends on the uncoupled parameters. Its dependency on d is lumped in the factors between brackets in (14) and (15). Separating the different effects and contributions, renders the analysis simpler [compare with (22)–(26)].

When d is very small ($k_2 d \ll 1$), the field of the $TE_{01\delta}^{++++\cdots}$ deviates significantly from that of the $TE_{01\delta}$ mode. Based on ECMT-I this can be explained by noticing that the smaller the spacing d between the conductors, the larger the effect of the mirror images. From Figs. 8 and 9, it is clear that for $d =$ 3.15 mm the PMC walls have a more profound effect. This is

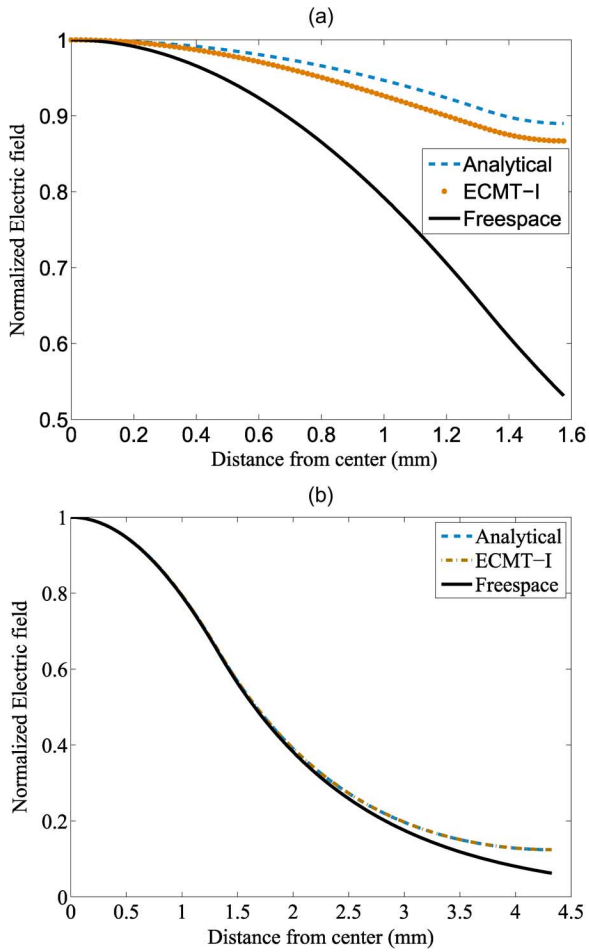

Fig. 9. Dielectric resonator sandwiched between two PMC plates: The normalized electric field calculated over $z \in [0, d/2]$. The distance between the two plates d is (a) 3.15 mm and (b) 8.65 mm.

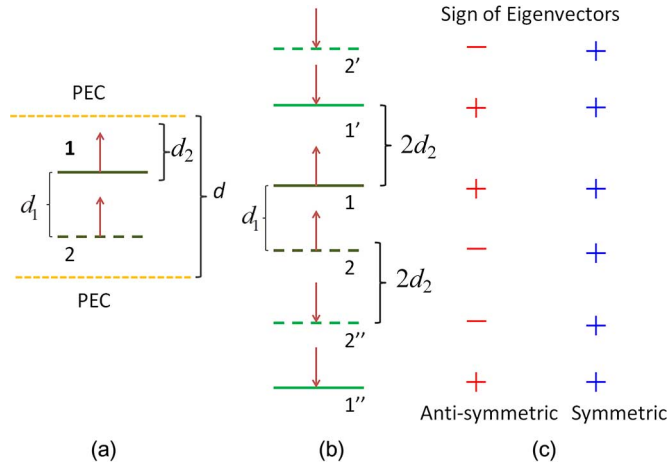

Fig. 10. (a) Two dielectric resonators separated by a distance of d_1 mm apart. Both resonators are d_2 away from PEC walls. (b) Equivalent coupled resonators images. (c) Phase shift of the symmetric and the anti-symmetric modes.

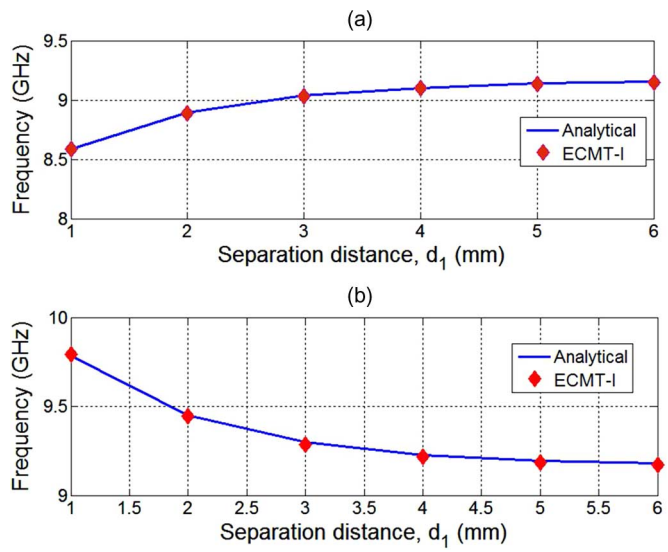

Fig. 11. Frequency of $|-\mathcal{R}-\mathcal{R}-|$ when $d_2 = 3$ mm. (a) Symmetric mode. (b) Anti-symmetric mode.

due to the fact that, for PMC walls, *all* the images' modes are in phase with the uncoupled mode (Zeroth order). Thus, the effect of $\hat{\mathbf{E}}$ is to enhance $\mathbf{E}_0$. On the contrary, the presence of the PEC walls, as shown in Fig. 4, alternates the phase between consecutive resonators, which makes the effect of the walls less profound. Quantitatively, the effect of the walls appears in the terms inside the brackets of (14) and (15). For $|-\mathcal{R}-|$ this term approaches 1/2, for small d values. On the other hand, the term gets substantially large (approaches $1/k_2 d$) when PMC walls are present.

The last system examined here is that of two dielectric resonators sandwiched between two PEC walls ($|-\mathcal{R}-\mathcal{R}-|$) and is shown in Fig. 10. In general, the two resonators' modes couple which result in symmetric and anti-symmetric modes. Because the two resonators are independent, the phase relation between the two real resonators modes [denoted by 1 and 2 in Fig. 10(a)]can be arbitrarily chosen. In the following analysis, the two modes were chosen to be in phase. As in the case of one resonator sandwiched between two conducting plates, the number of images is infinite. Due to the presence of two resonators, the 1st image order consists of four resonators. The phase relations of the images are dependent on the walls type. The arrows in Fig. 10(b) show the relative phase when PEC walls are used. Unlike the approximation used to determine the modes of $|-\mathcal{R}-|$, the full eigenvalue problem [15] is solved up to the 1st order images only. This is a 6×6 system resulting in six eigenvectors. However, due to the presence of two independent resonators, only two eigenvectors correspond to the physical system depicted in Fig. 10(a). Dictated by the method of images, the sign of the a coefficients of the image resonators always follow the real ones. (By referring to Fig. 10(b), the sign of the a coefficients of $1'$ and $1''$ follow that of 1. Similarly, the sign of the a coefficients of $2'$ and $2''$ follow that of 2). Thus, one ends up with two eigenvectors which have the sign relations shown in Fig. 10(c). In Fig. 3, d_2, the distance between the resonators and the PEC walls, is fixed to 3 mm and d_1, the distance between the two resonators, changes from 1 to 6 mm. Shown in Fig. 11 is the frequency of both the symmetric and anti-symmetric modes. The frequency is calculated using ECMT-I and the analytical model obtained in [10]. Because the full eigenvalue problem in [15] is solved, the coupling between all six

resonators and the coupling-induced frequency shifts terms are automatically taken into account. Although the first-order resonators are only used, ECMT-I can accurately calculate the frequencies of both coupled modes. This is true even when d_1 is small. This suggests that taking into account the coupling-induced frequency shift terms and the coupling with relatively far resonators improve the results.

It is worth noticing that provided that the fields and frequencies of the uncoupled resonators are known or estimated, ECMT-I can be applied to more complex systems where an analytical model is not possible or very complex. For example instead of using dielectric resonators, split-rings, loop gaps or capacitively loaded coils can be used.

IV. Conclusion

Using the method of images, the domain of ECMT was extended to cover cases where resonators are in the proximity of conductors. Because ECMT is in the form of an eigenvalue problem in the frequency domain, the extension can be easily achieved. It was shown that the type of conductors (PEC or PMC) and the orientation of the resonators with respect to them determine the phase of the images and consequently the sign of the coupling coefficient κ. This in turn determines whether the resonant frequency is increased or decreased. To verify the validity of the new approach, two cases were theoretically and numerically analyzed.

Appendix

For the $|-\mathcal{R}-|$ and $\sqsubset -\mathcal{R}- \sqsupset$ structures, the modes can be determined after solving the auxiliary Helmholtz's equation

$$\nabla^2\psi + k_0^2\psi = 0 \tag{16}$$

where $k_0 = \omega/c$, c is the speed of light. One is interested in the azimuthal independent symmetric solution of (16). The general solution is

$$\psi = J_0(k_\rho r)\begin{cases}\cos k_1 z, & |z| \le \frac{h}{2}\\ a\sinh k_2 z + b\cosh k_2 z, & |z| > \frac{h}{2}\end{cases} \tag{17}$$

where $k_\rho = 2.405/r_d$, r_d is the dielectric radius, $k_1 = \sqrt{\epsilon_r k_0^2 - k_\rho^2}$, and $k_2 = \sqrt{k_\rho^2 - k_0^2}$.

For $TE_{01\delta}$ like modes, $E_\rho = 0$, $H_\phi = 0$, $E_\phi = \partial\psi/\partial\rho$ and $H_\rho = (1/i\omega\mu_0)(\partial^2\psi/\partial\rho\partial z)$. The continuity of the fields across the boundaries can be written as

$$\begin{pmatrix}\cos(k_1h/2) & -\cosh(k_2h/2) & -\sinh(k_2h/2)\\ k_1\sin(k_1h/2) & k_2\sinh(k_2h/2) & k_2\cosh(k_2h/2)\\ 0 & \cosh(k_2d/2) & \sinh(k_2d/2)\end{pmatrix}\begin{pmatrix}1\\ a\\ b\end{pmatrix} = \mathbf{0} \tag{18}$$

for $|-\mathcal{R}-|$ and

$$\begin{pmatrix}\cos(k_1h/2) & -\cosh(k_2h/2) & -\sinh(k_2h/2)\\ k_1\sin(k_1h/2) & k_2\sinh(k_2h/2) & k_2\cosh(k_2h/2)\\ 0 & \sinh(k_2d/2) & \cosh(k_2d/2)\end{pmatrix}\begin{pmatrix}1\\ a\\ b\end{pmatrix} = \mathbf{0} \tag{19}$$

for $\sqsubset -\mathcal{R}- \sqsupset$. The resonant frequency is determined from (18) and (19) by solving the following transcendental equations:

$$\tan(k_1h/2) = \frac{k_2}{k_1}\cdot\frac{1}{\tanh(k_2(d-h)/2)} \tag{20}$$

for $|-\mathcal{R}-|$ and

$$\tan(k_1h/2) = \frac{k_2}{k_1}\tanh\left(k_2(d-h)/2\right) \tag{21}$$

for $\sqsubset -\mathcal{R}- \sqsupset$.

The electric field is found to be

$$\mathbf{E} = -k_\rho J_1(k\rho r)\begin{cases}\cos k_1 z, & |z| \le \frac{h}{2}\\ a\sinh k_2 z + b\cosh k_2 z, & |z| > \frac{h}{2}\end{cases} \tag{22}$$

For $|-\mathcal{R}-|$

$$a = \frac{\tanh(k_2d/2)}{\tanh(k_2d/2) - \tanh(k_2h/2)}\cdot\frac{\cos(k_1h/2)}{\cosh(k_2h/2)} \tag{23}$$

and

$$b = \frac{1}{\tanh\left(k_2d/2\right) - \tanh(k_2h/2)}\cdot\frac{\cos(k_1h/2)}{\cosh(k_2h/2)}. \tag{24}$$

For $\sqsubset -\mathcal{R}- \sqsupset$

$$a = \frac{\cos(k_1h/2)}{\cosh(k_2h/2) - \sinh(k_2h/2)\tanh(k_2d/2)} \tag{25}$$

and

$$b = \frac{\cos(k1h/2)}{\sinh(k_2h/2) - \cosh(k_2h/2)\coth(k_2d/2)}. \tag{26}$$

Acknowledgment

The authors would like to thank CMC Microsystems for providing HFSS that facilitated this research.

References

[1] S. S. Xiaofang Yu, S. Beiker, R. Sassoon, and S. Fan, "Wireless energy transfer with the presence of metallic planes," *Appl. Phys. Lett.*, vol. 99, no. 21, 2011, Art. ID 214102.

[2] X. Yu, T. Skauli, B. Skauli, S. Sandhu, P. B. Catrysse, and S. Fan, "Wireless power transfer in the presence of metallic plates: Experimental results," *AIP Advances*, vol. 3, no. 6, 2013, Art. ID 062102.

[3] R. Marqus, J. Martel, F. Mesa, and F. Medina, "Left-handed-media simulation and transmission of EM waves in subwavelength split-ring-resonator-loaded metallic waveguides," *Phys. Rev. Lett.*, vol. 89, no. 18, 2002, Art. ID 183901.

[4] T. Ueda, A. Lai, and T. Itoh, "Demonstration of negative refraction in a cutoff parallel-plate waveguide loaded with 2-D square lattice of dielectric resonators," *IEEE Trans. Microw. Theory Techn*, vol. 55, no. 6, pp. 1280–1287, Jun. 2007.
[5] G. Rinard and G. Eaton, "Loop-Gap Resonators," in *Biomedical EPR Part B: Methodology Instrumentation, Dynamics, Biological Magnetic Resonance*, S. Eaton, G. Eaton, and L. Berliner, Eds. New York, NY, USA: Springer, 2005, vol. 24/B, pp. 19–52.
[6] J. R. Anderson, R. A. Venters, M. K. Bowman, A. E. True, and B. M. Hoffman, "ESR and ENDOR applications of loop-gap resonators with distributed circuit coupling," *J. Magn. Res.*, vol. 65, no. 0022–2364, pp. 165–168, 1985.
[7] S. Y. Elnaggar, R. Tervo, and S. M. Mattar, "Coupled modes, frequencies and fields of a dielectric resonator and a cavity using coupled mode theory," *J. Magn. Res.*, vol. 238, no. 1090–7807, pp. 1–7, 2014.
[8] S. Y. Elnaggar, R. Tervo, and S. M. Mattar, "General expressions for the coupling coefficient, quality and filling factors for a cavity with an insert using energy coupled mode theory," *J. Magn. Res.*, vol. 242, no. 1090–7807, pp. 57–66, 2014.
[9] S. Y. Elnaggar, R. Tervo, and S. M. Mattar, "Optimal dielectric and cavity configurations for improving the efficiency of electron paramagnetic resonance probes," *J. Magn. Res.*, vol. 245, no. 1090–7807, pp. 50–57, 2014.
[10] S. Fiedziuszko and A. Jelenski, "The influence of conducting walls on resonant frequencies of the dielectric microwave resonator," *IEEE Trans. Microw. Theory Techn*, vol. MTT-9, no. 19, pp. 778–779, Sep. 1971.
[11] S. Fiedziuszko and A. Jalenski, "Double dielectric resonator," *IEEE Trans. Microw. Theory Techn*, vol. MTT-19, no. 9, pp. 779–781, Sep. 1971.
[12] Y. E. Nesmelov, J. T. Surek, and D. D. Thomas, "Enhanced EPR sensitivity from a ferroelectric cavity insert," *J. Magn. Res.*, vol. 153, no. 1090–7807, pp. 7–14, 2001.
[13] S. B. Cohn, "Microwave bandpass filters containing high-Q dielectric resonators," *IEEE Trans. Microw. Theory Techn*, vol. MTT-16, no. 4, pp. 218–227, Apr. 1968.
[14] F. Zhang, Q. Zhao, J. Sun, J. Zhou, and D. Lippens, "Coupling effect of split ring resonator and its mirror image," *Pr. Electromagn. Res.*, vol. 124, pp. 233–247, 2012.
[15] S. Y. Elnaggar, R. Tervo, and S. M. Mattar, "Energy coupled mode theory for electromagnetic resonators," *IEEE Trans. Microw. Theory Techn*, accepted for publication.
[16] R. F. Harrington, *Time-Harmonic Electromagnetic Fields*. New York, NY, USA: McGraw-Hill, 1961.
[17] J. Sheen, "Study of microwave dielectric properties measurements by various resonance techniques," *Measurement*, vol. 37, no. 0263–2241, pp. 123–130, 2005.
[18] W. C. Yueh, "Eigenvalues of several tridiagonal matrices," *Appl. Math. E-Notes*, vol. 5, pp. 66–74, Apr. 2005.
[19] D. Sievenpiper, Z. Lijun, R. F. J. Broas, N. G. Alexopolous, and E. Yablonovitch, "High-impedance electromagnetic surfaces with a forbidden frequency band," *IEEE Trans. Microw. Theory Techn*, vol. 47, no. 11, pp. 2059–2074, Nov. 1999.
[20] R. R. Mett, J. W. Sidabras, I. S. Golovina, and J. S. Hyde, "Dielectric microwave resonators in TE011 cavities for electron paramagnetic resonance spectroscopy," *Rev. Sci. Instrum.*, vol. 79, no. 9, p. 94702, 2008.
[21] S. M. Mattar and S. Y. Elnaggar, "Analysis of two stacked cylindrical dielectric resonators in a TE102 microwave cavity for magnetic resonance spectroscopy," *J. Magn. Res.*, vol. 209, no. 1090–7807, pp. 174–182, 2011.
[22] M. Popovic, C. Manolatou, and M. Watts, "Coupling-induced resonance frequency shifts in coupled dielectric multi-cavity filters," *Opt. Exp.*, vol. 14, no. 3, pp. 1208–1222, 2006.
[23] D. M. Pozar, *Microwave Engineering*, 2nd ed. Hoboken: John Wiley and Sons, 2005.
[24] I. Awai and Y. Zhang, "Coupling coefficient of resonators-An intuitive way of its understanding," *Electron. Commun. Japan*, vol. 90, no. 9, pp. 11–18, 2007.

Sameh Y. Elnaggar received the B.Sc. and M.Sc. degrees in electrical engineering from Alexandria University, Alexandria, Egypt, in 2000 and 2006, respectively, and the Ph.D. degree in electrical and computer engineering from the University of New Brunswick, Fredericton, NB, Canada, in 2013.

His recent research interests are in computational electromagnetic, interferometry, magnetic resonance, quasi-optics, metamaterials, and wireless power transfer. He is currently with School of Engineering and Information Technology, University of New South Wales, Canberra, Australia.

Richard J. Tervo received the B.Sc. degree in physics and M.Sc. degree in experimental nuclear physics from McMaster University, Hamilton, ON, Canada, in 1980 and 1982, respectively, and the Ph.D. degree in electrical engineering from Laval University, Quebec, QC, Canada, in 1988.

He joined the Department of Electrical and Computer Engineering, University of New Brunswick, Fredericton, NB, Canada, in 1986. His research interests include digital systems, instrumentation, communications and signal processing.

Saba M. Mattar received the B.Sc. degree in chemistry and physics from Alexandria University, Alexandria, Egypt, in 1968, the M.Sc. degree in solid-state science from The American University, Cairo, Egypt, in 1974, and the Ph.D. degree in chemistry from McGill University, Montreal, QC, Canada, in 1982.

He joined the Chemistry Department, University of New Brunswick, Fredericton, NB, Canada, in 1986, where he is presently an Honorary Research Professor. His interests are theoretical and experimental magnetic resonance, trapping of reactive intermediates, electronic structure of molecules, chemical physics, new metamaterials, spectroscopy, and instrumentation.